Pd-based metallic supported membranes : high temperature stability and fluidized bed reactor testing

Available online at www.sciencedirect.com

ScienceDirect

journal homepage: www.elsevier.com/locate/he

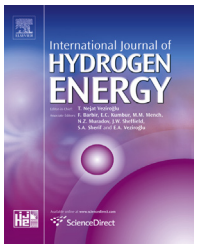

Pd-based metallic supported membranes: High-temperature stability and fluidized bed reactor testing

Jose Antonio Medrano [a], Ekain Fernandez [a,b], Jon Melendez [b,c], Maria Parco [b], David Alfredo Pacheco Tanaka [b], Martin van Sint Annaland [a], Fausto Gallucci [a,*]

[a] Chemical Process Intensification, Department of Chemical Engineering and Chemistry, Eindhoven University of Technology, Den Dolech 2, 5612AD Eindhoven, The Netherlands

[b] TECNALIA, Energy and Environment/Industry and Transport Divisions, Mikeletegi Pasealekua 2, 20009 San Sebastián-Donostia, Spain

[c] Chemical Engineering and Environmental Department, University of The Basque Country UPV/EHU, C/ Alameda Urquijo s/n, 48013 Bilbao, Spain

ARTICLE INFO

Article history:
Received 11 September 2015
Received in revised form
16 October 2015
Accepted 23 October 2015
Available online 12 November 2015

Keywords:
Palladium membrane
Metallic support
Membrane stability
Fluidized bed membrane reactor
Autothermal steam reforming

ABSTRACT

The present work focuses on the study of a metallic supported Pd–Ag membrane for high temperature applications with a particular attention to long-term stability. In this work, a metallic supported thin-film Pd–Ag membrane has been tested for more than 800 h and sustained hydrogen perm-selectivities higher than 200000 have been measured. Furthermore, it has been demonstrated that there is no interaction of the membrane with the Ni/$CaAl_2O_4$ reforming catalyst particles, thus resulting in a constant permeance in the fluidized bed membrane reactor mode. The membrane has been tested under steam and autothermal reforming of methane conditions and the membrane performance has been quantified in terms of the hydrogen recovery and separation factors demonstrating a good reactor performance accomplishing an enhancement in the process efficiency by in-situ selective H_2 separation. A decrease in ideal perm-selectivity has been observed at high temperatures (600 °C). Small defects at the Pd/Ag surface as a result of interaction of the Pd/Ag later with the metallic support have been observed in after test membrane characterization, which provides appreciated information for the improvement in the performance and production of future membranes.

Introduction

Global warming and scarcity of resources are the two main issues that need to be addressed in energy conversion processes. Nowadays, there are many reports and reviews with extensive discussions on these issues and also different strategies have been proposed to mitigate the associated problems [1]. While most of the strategies are related to the use of renewable resources or moving towards clean energy "sources" like H_2, what it is generally accepted nowadays is

* Corresponding author.
E-mail address: f.gallucci@tue.nl (F. Gallucci).

http://dx.doi.org/10.1016/j.ijhydene.2015.10.094

that a transition to these novel strategies should be done through improved energy efficiency of existing technologies.

Large-scale hydrogen production is nowadays based mostly on reforming of fossil fuels (mainly natural gas) or, for small plants and high purity, electrolysis of water. For hydrogen production processes based on reforming one of the major drawbacks is the large amount of CO_2 emissions. These emissions depend on the process configuration used for the reforming as well as the feedstock. To reduce these emissions CH_4 is the preferred raw material for H_2 production related to the high H/C ratio [2]. Among the different reforming processes, Steam Methane Reforming (SMR) is the most employed process to convert CH_4 into H_2. This is a highly endothermic process where the reforming reaction is usually carried out over a nickel catalyst for syngas production, which is subsequently sent to water-gas-shift reactors. Typical temperatures for the process at large-scale range between 800 and 1100 °C with the necessity of an excess of steam in the feed (typically with a steam-to-carbon ratio (S/C) around 3) to avoid carbon deposition on the surface of the catalyst [3]. To supply the heat needed for the highly endothermic reforming, part of the feed is combusted in a burner. Autothermal Methane Reforming (ATR) is another well-known process for H_2 production, where some oxygen is fed to the reactor with the aim of obtaining autothermal operation via partial oxidation of the fuel. In this process, the main limitation is associated to the expensive separation of oxygen from air [4]. Other processes for H_2 production are based on dry reforming or partial oxidation of methane. The main drawback of these processes is related to the relatively low H_2/CO ratio in the obtained syngas, which makes them less attractive for large-scale industrial applications [5,6]. Thus, SMR and ATR are the main processes of interest for H_2 production from natural gas.

In view of the desired transition to novel carbon-emission-free based technologies for energy production, an improvement in the overall carbon and energy efficiencies of current processes is of crucial importance, which has led to a lot of research efforts in many research institutes and universities. Regarding SMR and ATR processes, main efforts have been devoted to the development of novel, more stable catalysts with high resistance to carbon deposition and/or sulfur poisoning [7]. However, what it is gaining more attention nowadays is the development of novel reactor concepts for efficient reforming technologies. Among them, the use of membrane reactors has been proposed and demonstrated at lab scale as an interesting alternative to the traditional processes. In a membrane reactor, chemical reaction and separation take place in the same unit, thus achieving an important process integration which accomplishes a reduction in the required number of process units even when aiming for CO_2 capture [8–10].

Perovskite membranes have been used in ATR processes to separate oxygen from air for selective (and distributive) feeding of O_2 to the reactor. By using these membranes costly air separation units are no longer required and a better control of the process can be achieved. The main limitation associated with the application of these membranes in ATR processes is that the O_2 permeation rates become sufficient only at very high temperatures [11]. The use of Pd-alloys membranes is another interesting option for membrane reactors, where selective H_2 separation can be achieved *in situ*. In this case, product separation results in a displacement of the thermodynamic equilibrium, so that higher feedstock conversions can be achieved with an integrated separation (and purification) of the H_2 produced, which is otherwise carried out at industrial scale with PSA units. In this case, the main limitation is related to the maximum temperature the Pd-based membranes can resist, which is currently around 600 °C, and to a lesser extent the inhibition by CO, which reduces the H_2 flux through the membrane [12,13]. Membrane reactors have been studied mostly considering a packed-bed reactor configuration [14,15]. However, after enormous efforts in developing novel thin-film Pd-based supported membranes with a very high H_2 permeance (with simultaneously a very high H_2 perm-selectivity), many drawbacks of the packed-bed membrane reactor configuration have emerged, most of them are associated to bed-to-membrane mass transfer limitations, commonly referred to as concentration polarization [16,17]. Moreover, the relatively large pressure drop in fixed bed membrane reactors can be circumvented by employing bigger particles, however, at the expense of possible intra-particle mass transfer limitations. Finally, temperature control in packed bed reactors may be problematic (especially for highly endo or exothermic reactions) with very limited freedom for different membrane and heat exchange arrangements [18].

All the drawbacks of packed-bed membrane reactors may be alleviated with fluidized bed membrane reactors [19]. While concentration polarization and temperature gradients can be largely reduced in fluidized beds, it has also been shown that stability issues related to attrition of the catalyst particles or erosion of the membrane surfaces may not pose any problems or can be overcome [20].

Concerning the Pd-based supported membranes, metallic supports are more robust than ceramic supports and there is no need of sealing, provided that an appropriate welding between the porous and dense parts can be performed [21]. For high temperature applications using metallic supported membranes, the deposition of an inter-metallic diffusion barrier layer between the metallic support and the Pd-based layer is required [18]. Recently, the long-term stability of Pd-based membranes at temperatures above 450 °C has become a key research challenge, since the membranes showed loss of performance due to alloying of Pd with the support elements, Ag sublimation in the case of Pd–Ag membranes, grain growth or problems associated with the membrane preparation procedure [16,22–26].

In this study Pd–Ag membranes supported on metallic Hastelloy X tubes with a ceramic inter-metallic diffusion barrier layer have been prepared and their performance in a fluidized bed reactor for SMR and ATR reactions has been studied. Firstly, the long-term membrane stability is assessed and the influence of CO on membrane inhibition is evaluated at different temperatures and partial pressures. Subsequently, the membrane is immersed in a fluidized catalytic bed with a commercial Ni/$CaAl_2O_4$ catalyst (HiFUEL® R110) provided by Johnson Matthey, which has already demonstrated good performance for low temperature reforming applications as described in Ref. [27]. A continuous monitoring of the membrane properties is carried out after every step described in

this study. Finally, once all experimental work is concluded, a deep characterization of the membrane is carried out for further optimization of the membranes.

Experimental

Membrane preparation and characterization

Metallic supported membranes were prepared at TECNALIA for the tests presented in this work. A Hastelloy X porous tube (3/8″ o.d.; 0.2 μm media grade) supplied by Mott Corporation was used as membrane support. For this application, the tube was first surface treated by Mott Corp. consisting on grounding and reactivating steps obtaining smaller surface pores and lower surface roughness. Then, various Al_2O_3-YSZ ceramic layers were deposited and sintered by wet deposition techniques [21] in order to provide the inter-metallic diffusion barrier layer. Finally, thin Pd–Ag layers were deposited by using the simultaneous (Pd and Ag) electroless plating technique reported in Ref. [28]. The membrane was prepared with a base plating process (210 min) and a second plating step (90 min). After each plating step, the membrane layers were annealed at 650 °C for 2 h; which is above the maximum operating temperature for the ATR membrane reaction (ca. 600 °C), by exposing the membrane to a 10% H_2/90% N_2 gas mixture with the same heating rate and gas flow rates as reported previously [29]. A picture of the final membrane is shown in Fig. 1 and a SEM cross-section image of the membrane in Fig. 2, where the treated support, ceramic inter-layer and Pd–Ag layer can be identified.

After test membrane characterization has been carried out with different techniques. The cross-section of the membrane and its surface were analyzed with a JEOL JSM-6330F SEM-EDX equipment. Before the analysis, for proper inspection of the cross-section of the membrane, metallographic specimens were prepared mounting membrane pieces in bakelite and polishing them.

The composition in the surface in order to identify all possible elements has been analyzed by means of an X-ray photo-electron spectroscopy (XPS). Data were recorded on a Kratos AXIS Ultra spectrometer equipped with a monochromatic AlKα X-ray source and a delay-line detector (DLD). Spectra were obtained using an aluminium anode (hv = 1486.6 eV) operating at 150 W, with survey scans at constant pass energy of 160 eV and region scans at a constant pass energy of 40 eV. The background pressure was $2 \cdot 10^{-9}$ mbar. CasaXPS data processing software was used for peak fitting and quantification, where all binding energies were referenced to the C 1s line at 284.6 eV. The surface composition was estimated from the integrated intensities corrected by the atomic sensitivity factors.

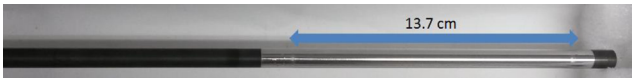

Fig. 1 – Metallic supported membrane welded to dense Inconel 600 tubes.

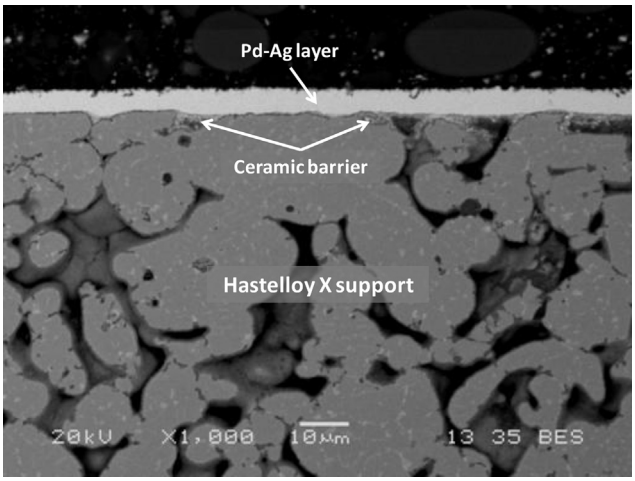

Fig. 2 – Cross-section SEM image of a ~5 microns thick Pd–Ag membrane supported on ceramic coated Hastelloy X porous tube [21].

Membrane permeation characterization

The metallic supported membrane was characterized in a membrane permeation test equipment that can be used for testing the permeation properties of the membranes using single gases, simulated mixtures of gases and also in reactive conditions with fluidized catalyst. A shell-and-tube module configuration has been used to test the membranes. The module is centered in an oven with three zones temperature controllers. The feed flow rate was controlled by digital mass flow controllers and the steam by a CEM system (Bronkhorst). The pressure in the reactor was controlled with a back-pressure regulator after steam condensation. The flow rate of the permeate and retentate streams was monitored by Brooks mass flow meters. To determine the N_2 leakage a Bronkhorst flowmeter has been used (model F-110C-002; Nominal flow: 0.014–2 Nml/min Air). To enhance the driving force for hydrogen permeation, the test rig is equipped with a vacuum pump for hydrogen (ATEX certified). The PFD for the Reforming Test Setup is shown in Fig. 3.

Long-term single gas permeation tests at high temperatures

Before the membrane is tested under reactive conditions, it is important to assess its stability as a function of time on stream. While sealing issues are solved by using metallic supports instead of ceramics, the possible interaction between the Pd–Ag alloy and the support must be evaluated. For this purpose, stability tests have been carried out in the experimental setup described in Fig. 3.

Prior to the stability test, the reactor is heated up with a heating rate of 2 °C/min in a N_2 atmosphere and 1 bar, until the selected temperature is reached. Single gas tests for H_2 and N_2 are performed every day in order to evaluate the ideal H_2/N_2 permselectivity as a function of time on stream. While the H_2 permeation rate was measured with a Horibastec film flow meter, the N_2 permeation was measured with a Bronkhorst flowmeter with a precision of 0.01 mL/min in view of the very low flow rates. Stability tests have been carried out at different

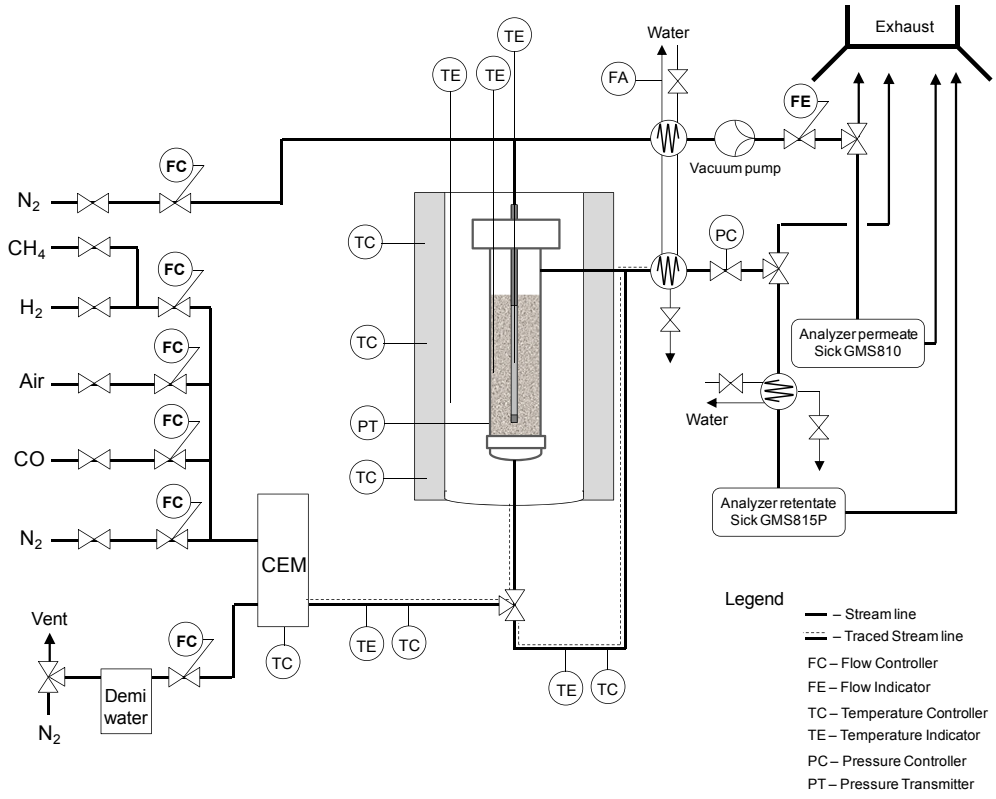

Fig. 3 – PFD of reformer setup used for membrane tests for high temperature application.

operating temperatures with a temperature stepwise increase of 25 °C once the H_2 permeation became stable with time on stream. In total, the membrane has been exposed to high temperature and H_2 permeation for more than 800 h.

Mixed gas membrane permeation tests (influence of CO)

It is known that CO is adsorbed on the Pd causing an important decrease in the H_2 permeation associated to a decrease in the effective surface area available for H_2 permeation [29–31]. Therefore, it is important to study the influence of the presence of CO on the H_2 permeation. This effect is more pronounced at lower temperatures and it increases with an increase in the CO feed concentration. For this test, different mixtures of H_2/N_2 and H_2/CO have been used in order to quantify the CO inhibition effect for similar partial pressures of H_2 at the feeding side. The temperature has been varied from 400 °C to 600 °C for CO concentrations of 5, 7.5, 10 and 15% (v/v). For these tests, the CO concentration at the permeate side is measured with a Sick Analyzer connected to the permeate side, able to measure the CO and CO_2 concentration in the range of ppm to obtain the H_2 volume fraction in the permeate stream. For a good comparison, all the results have been normalized with the actual partial pressure of H_2 at the reactor side.

Tests under reforming conditions in a fluidized bed reactor

After single gas tests without the presence of a solids phase, the reactor has been filled with 300 g of a commercial NiO/$CaAl_2O_4$ catalyst provided by Johnson Matthey with a particle size ranging between 150 and 250 μm, completely submerging the membrane. Separate attrition tests have shown that the catalyst is not damaged when used under fluidization conditions; in particular, the particle size distribution does not change either after 24 h of cold fluidization or 24 h of fluidization at 600 °C. Prior to all experimental evaluation under reactive conditions, the minimum fluidization velocity of the solids phase has been experimentally measured with the pressure-drop method at a value of 0.012 m/s at 500 °C with N_2 as fluidizing gas. The heating up procedure of the system is carried out with 2 °C/min under N_2 atmosphere until the desired temperature was reached. Once at high temperatures, the possible interaction between the surface of the membrane and the catalyst is analyzed by comparing the H_2 permeance with single gas test results without the catalyst bed for the same conditions.

Steam Methane Reforming (SMR) and Autothermal Reforming of Methane (ATR) were carried out in this system. For both cases a reference case with a steam-to-carbon ratio (S/C) of 3, a temperature of 500 °C, 4 bar absolute pressure inside the reactor and 10% mole fraction of methane in the inlet gas has been selected. For the case of autothermal reforming, some oxygen is added with the inlet gas in order to have an oxygen-to-carbon ratio (O/C) of 0.25. In all cases N_2 is used as internal standard for analyzing the carbon balance. The influence of different parameters has been studied for both reaction systems. All the details concerning the experiments performed in the reactor have been summarized in Table 1.

Table 1 – Experimental conditions for tests performed in the fluidized bed reactor setup.

Parameter	Reference case	Conditions tested
Steam methane reforming (SMR)		
Temperature (°C)	500	500–600
Inlet pressure (bar)	4	2–5
Steam-to-carbon ratio (S/C)	3	2–4
Inlet flow rate (L/min)	4.4	3.5–5.2
CH_4 inlet composition (%v/v)	10	Not varied
Autothermal reforming of methane (ATR)		
Temperature (°C)	500	500–600
Inlet pressure (bar)	4	2–5
Steam-to-carbon ratio (S/C)	3	2–4
Inlet flow rate (L/min)	4.4	3.5–5.2
CH_4 inlet composition (%v/v)	10	Not varied
Oxygen-to-carbon ratio (O/C)	0.25	Not varied

Results and discussion

For all cases the results have been expressed in terms of methane conversion, the hydrogen recovery factor (HRF) and the separation factor (SF) (Equations (1)–(3)). While the methane conversion gives information about the global process and performance of the catalyst, the other two parameters are directly associated to the performance of the membrane. HRF is an indication of the amount of H_2 permeated through the membrane relative to the maximum amount of hydrogen that could be produced at full conversion. SF provides information on the amount of hydrogen permeated relative to the total amount of hydrogen produced. Thus, a higher membrane permeance will result in higher HRF and SF values at otherwise the same conditions.

- Methane conversion: $X_{CH_4} = \frac{\varnothing_{CH_4.in} - \varnothing_{CH_4.out}}{\varnothing_{CH_4.in}}$ (1)
- Hydrogen recovery factor: $HRF = \frac{\varnothing_{H_2.permeated}}{4 \cdot \left(\varnothing_{CH_4.in} - \frac{1}{2}\varnothing_{O_2.in}\right)}$ (2)
- Separation factor: $SF = \frac{\varnothing_{H_2.permeated}}{\varnothing_{H_2.total}}$ (3)

Long-term single gas permeation test results

The membrane stability has been assessed between 500 and 600 °C for around 800 h. The main aim of this test is to check the stability of the hydrogen permeance and the nitrogen leakage through the membrane as a function of time on stream. The results of this test are presented in Fig. 4. It can be concluded that the membrane shows a really good stability for hydrogen permeation during the whole test (~1.3×10^{-6} mol m^{-2} s^{-1} Pa^{-1}). However, at a certain temperature the hydrogen permeance slightly decreased over time, as also reported in the literature before for this type of membranes [23]. The nitrogen leakage through the metallic supported membrane was extremely low and even below the detection limit of the Bronkhorst flow meter (0.01 mL/min) for almost 800 h, which resulted in an ideal H_2/N_2 perm-selectivity higher than 200.000.

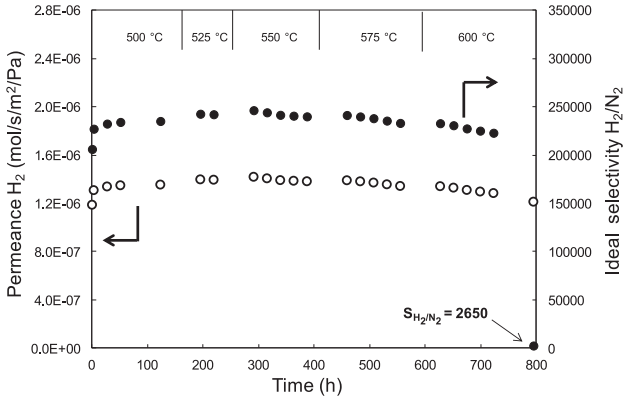

Fig. 4 – H_2 permeance (open circles) and H_2/N_2 ideal permselectivity (closed circles) of the metallic supported membrane as a function of time on stream at 500–600 °C.

The test was carried out at different temperatures with a stepwise increase of 25 °C. However, once at 600 °C and after 795 h of permeation tests, the nitrogen was permeating through the membrane resulting in a pronounced decrease in the ideal perm-selectivity which quickly dropped to a value of 2650. Nevertheless, this value of ideal perm-selectivity is still relatively high when compared to other state-of-the-art metallic supported membranes, as mentioned in Ref. [21]. The observed increase in N_2 permeation is investigated and explained later using results from after test characterization of the membrane.

Mixed gas permeation tests results (influence of CO and N_2 dilution)

The study of the effect of CO and N_2 dilution on the H_2 permeance through the membrane has been carried out just after the stability test for single gas permeation at different temperatures. Prior to this new test, the membrane has been exposed to a cooling-heating cycle to investigate whether there is a thermal stress affecting the permeance. The thermal cycle consisted of cooling the membrane to room temperature with a rate of 2 °C/min in N_2 atmosphere and subsequently heating up to the temperatures used for mixed gas permeation tests. The results in Fig. 5, where the effect of CO and N_2 dilution on the membrane permeation is shown, were obtained just after the heating-cooling cycle. In this case the maximum H_2 permeance achieved for a single gas test (black bars) is slightly lower than the last value measured from the long-term stability test. This implies that the membrane suffers from a small deactivation after a first heating-cooling procedure. Most probably this reduction is associated to a first thermal stress of the membrane with the consequent modification in the porosity of the support materials, thus increasing the mass transfer resistance through the supported membrane and decreasing the H_2 permeance. Coming back to the effect of CO and N_2 dilution on the hydrogen permeance,

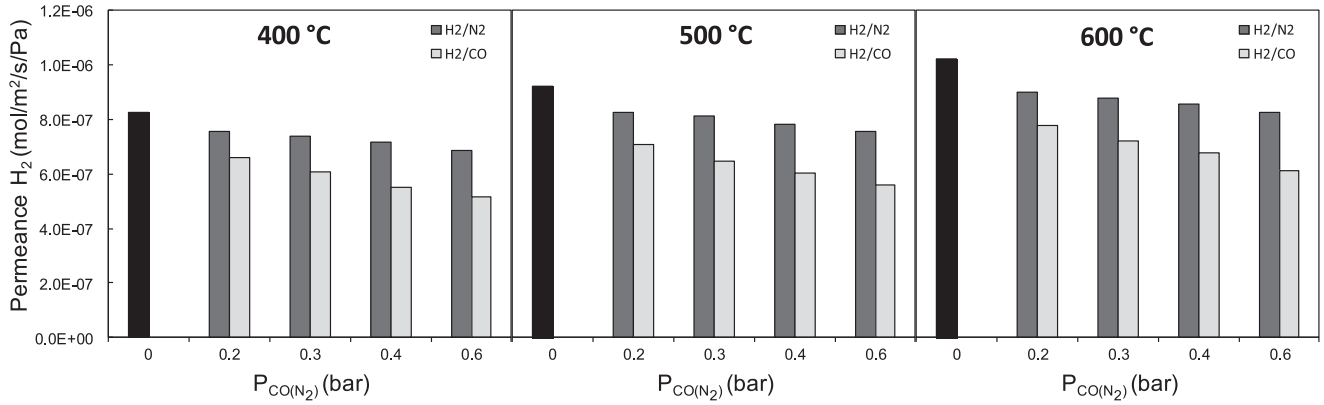

Fig. 5 – H_2 permeance as a function of partial pressure of CO (light grey bars) or N_2 (dark grey bars) at different temperatures. Black bars correspond to single gas tests with pure H_2. All experiments are carried out at a total pressure of 4 bar(a) in the reactor side and atmospheric pressure in the permeate side.

three different temperatures have been selected (400, 500 and 600 °C). For all cases the H_2 permeation has been normalized depending on the actual driving force. On a first close look on Fig. 5, it is clearly observed that when feeding another gas with H_2 at the inlet of the reactor at the same partial pressure of H_2, this gas creates an additional mass transfer resistance for hydrogen permeation through the membrane. This is concluded from the decrease in the H_2 permeance compared to the single gas test (black bars). Moreover, the higher the partial pressure of N_2, the lower the H_2 permeance for all investigated temperatures. As nitrogen does not interact with the membrane surface, the decrease in permeation fluxes is due to bulk-to-membrane mass transfer resistances.

When substituting N_2 for CO, a more pronounced decrease in H_2 permeance is observed for the same partial pressures of CO as the ones used before with N_2. In this case, the decrease is associated to poisoning of the surface by interaction of the Pd with CO. This interaction implies a decrease in the effective surface area available for H_2 permeation with its respective effect on the total gas permeation. Furthermore, it has been observed that an increase in the CO partial pressure implies a decrease in the H_2 permeance. This is in contrast with what has been reported in literature [31], where it was reported that at a certain CO concentration in the inlet stream (≈10% v/v) the H_2 permeance remains constant. As the difference between the permeation in the presence of CO and in the presence of N_2 increases with increasing the partial pressure of the gas component, this effect cannot be explained only by CO-inhibition and external mass transfer limitations (concentration polarization). These unexpected results can be explained by the catalytic activity of the support material (Inconel) towards methanation. Since this material contains mainly Ni, methanation may occur on the surface of the support forming CH_4. Through this reaction there is a decrease in the partial pressure of H_2 in the system, which is directly associated to a decrease in the H_2 permeation which explains why the H_2 permeance decreases further than expected in the presence of CO. To prove this hypothesis, the catalytic activity of the support has been tested by feeding a mixture (1 NL/min) of 25% H_2/25% CO in nitrogen at 500 °C and 1 bar and measuring the outlet composition. As reported in Fig. 6, indeed the support has activity towards methanation and the hydrogen concentration is indeed lower than the feed concentration, supporting the previous hypothesis.

Furthermore, it should be noted that this reaction will take place predominantly in highly concentrated H_2 streams and in the presence of CO, thus only at the permeate side and not significantly at the retentate side during SMR or ATR processes, as the reaction rates for SMR and ATR are much higher than methanation reaction rate. The observed methanation reactivity may even be advantageous when highly concentrated H_2 streams for industrial processes are required. Worth mentioning is the production of ultra-pure H_2 for usage in fuel cells for electricity production or in ammonia plants, where traces of CO have an important effect on the downstream processes [32], while the presence of CH_4 has a negligible influence. Thus, the fact that CO can be converted into CH_4 inside the membrane may have a positive impact on the quality of the H_2 stream produced. Thermodynamic calculations demonstrate that when traces of CO are present in the permeate stream these will be completely converted to methane as reported in Table 2.

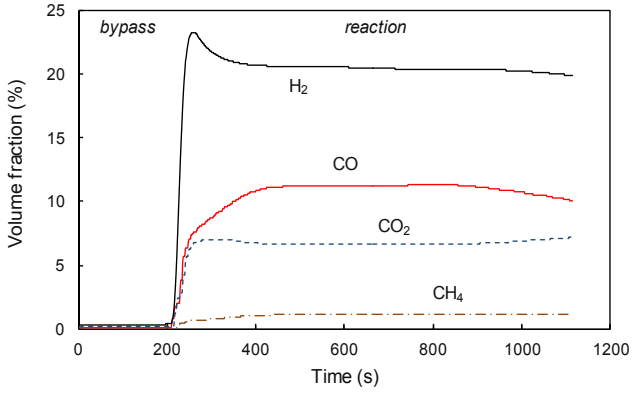

Fig. 6 – Reaction tests with the membrane support. T = 500 °C, p = 1 bar.

Table 2 – Thermodynamic calculations for the methanation reaction. Base for calculation is 1 kmol/h.

400 °C and 4 bar(a)		Inlet (kmol/h)	Outlet (kmol/h)
$P_{CO} = 0.2$ bar	CO	0.05	0
	CO_2	–	0
	CH_4	–	0.05
	H_2O	–	0.05
	H_2	0.95	0.8
$P_{CO} = 0.3$ bar	CO	0.075	0
	CO_2	–	0
	CH_4	–	0.075
	H_2O	–	0.075
	H_2	0.925	0.7

Test under reforming conditions

Steam methane reforming

The catalytic activity has been studied with the fluidized bed reactor configuration according to the experiments described in Table 1. For all cases, the reaction has first been carried out with the permeate side closed (i.e. avoiding permeation through the membranes thus simulating a conventional reactor without membranes). Steady state operation is reached within a few seconds after the start of the reaction. Sufficient data has been recorded during the steady state operation (around 20 min) and, after that, the permeate side is opened and the vacuum pump is connected in order to maximize the H_2 permeation through the membrane. For this new scenario a new steady state is observed corresponding with the displacement of the equilibrium as a consequence of the H_2 permeating through the membrane, which is also monitored during reaction. In order to obtain a good comparison of the results, a thermodynamic analysis using Aspen Plus V7.3.2 of the gas mixture with and without accounting for the amount of H_2 extracted, is also shown in the main figures presented below. For almost all cases it is observed that thermodynamic equilibrium is achieved in the fluidized bed reactor configuration (without membrane) and that, after changing the configuration to a fluidized bed membrane reactor, the conventional equilibrium restriction is circumvented, and the permeate outlet stream is again close to its thermodynamic equilibrium when accounting for the H_2 extracted.

Prior to the experiments, the membrane has been cooled down and the reactor was filled with 300 g of the catalyst in order to completely cover the membrane. Despite the observed decrease in H_2 permeance after a first thermal process, in this new case, when the whole system is heated up to the temperature for the reference case, the H_2 permeance remained almost constant with a value similar to the last measured during the test for CO inhibition. These details are summarized in Table 3, where the H_2 permeation and the ideal H_2/N_2 perm-selectivity at different moments in this study are summarized. These permeation results confirm that there is no interaction between the catalyst and the membrane.

The methane conversion as a function of different experimental conditions for the two different reactor configurations studied in this work is shown in Fig. 7. As can be observed, chemical equilibrium is obtained in the fluidized bed reactor configuration due to the good performance of the catalyst, assuring absence of kinetic limitations. Furthermore, for all cases an important increase in the yield of the reaction for H_2 production as a consequence of the displacement of the equilibrium is observed when the membrane reactor configuration is employed. It is especially interesting to highlight that the equilibrium displacement is more pronounced for conditions where the driving force for H_2 permeation is maximized, such as an increase in the pressure of the reactor and the steam-to-carbon ratio, or a decrease in the total flow rate with the corresponding increase in residence time. Under the new scenario with the configuration of the FBMR, the expected thermodynamic equilibrium has been also calculated with Aspen Plus. As observed from Fig. 7, again thermodynamic equilibrium is almost achieved in this new configuration. The difference observed might relate to the small amount of catalyst in the freeboard, which may not be enough to achieve the expected equilibrium. For all the cases studied in this work, a maximum error in the carbon balance of around 5–8% is obtained as a consequence of experimental errors mainly related to the analyzer calibration.

While the methane conversion for the different conditions may provide a quick visual interpretation on how well the membrane reactor performs, there are other parameters of interest that must be studied, mainly related to separation factor (SF) and hydrogen recovery factor (HRF). Both parameters give an indication on the H_2 recovered through the membrane as the maximum expected according to the inlet conditions and hydrogen produced. Both parameters are strongly affected by the driving force. Thus the amount of hydrogen produced during reaction and the amount of inert gas fed through the reactor play in important role on both parameters. Moreover, as observed during the CO inhibition experiments, there is a mass transfer resistance associated to the mixing of hydrogen with other gas components. This directly implies that the value of H_2 permeance will be far from the ideal value that was obtained during to single gas permeation tests.

Table 3 – Properties of the permeate side at different times during this study.

Case	H_2 permeance [$mol \cdot m^{-2} \cdot s^{-1} \cdot Pa^{-1}$]	Ideal H_2/N_2 selectivity [-]	Purity $H_{2,perm}$ [%]	CO, perm (ppm)	CO_2, perm (ppm)
Before SMR process	$8.69 \cdot 10^{-7}$	574.2	–	–	–
Reference case SMR	n/a	n/a	97.6	268.9	896.9
Between SMR and ATR processes	$8.67 \cdot 10^{-7}$	159.3	–	–	–
Reference case ATR	n/a	n/a	97.1	367.1	720.7
After ATR process	$8.77 \cdot 10^{-7}$	132.4	–	–	–

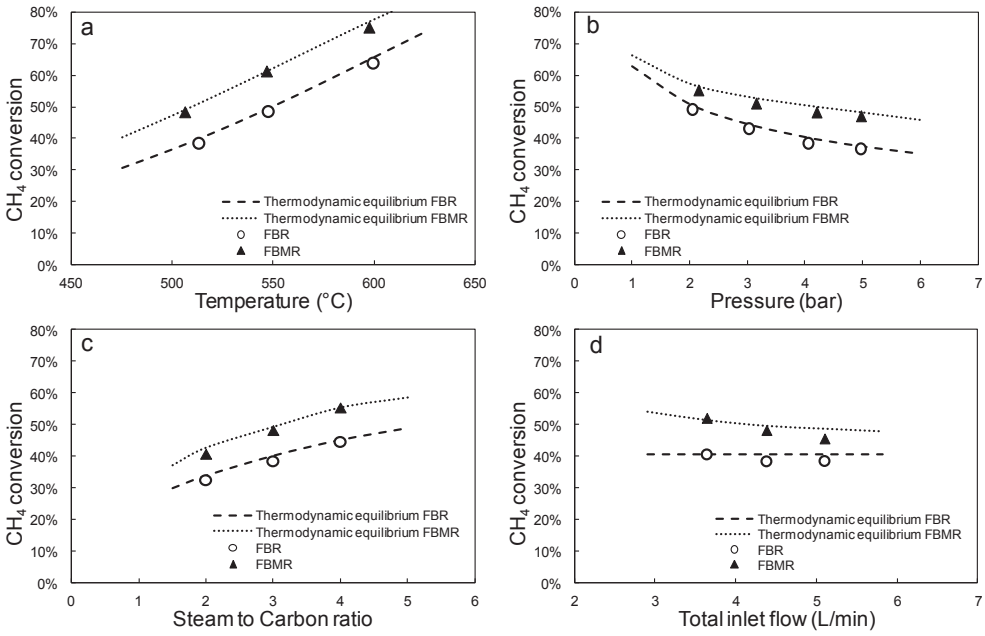

Fig. 7 – Methane conversion as a function of a) temperature, b) pressure, c) steam-to-carbon ration and d) inlet flow rate for the two reactor configurations studied with reference case conditions and the thermodynamic equilibrium for steam methane reforming calculated in Aspen Plus v7.3.2.

It is observed in Fig. 8 that both parameters are far from the ideal case of 100%. In order to interpret the results, it is important to first note that full conversion of CH_4 is never achieved and that for most of the investigated cases it never goes beyond 55%. This fact has as a consequence that high HRF cannot be achieved in this setup. Moreover, the huge amount of inert gas fed with the inlet composition (required for steam production) decreases dramatically the partial pressure of the other components. It has indeed an important effect on the maximum driving force that can be achieved for hydrogen separation. Furthermore, if this fact is combined with the mass transfer resistance for hydrogen permeation in the presence of other gases as discussed before, it results in a low separation factor (around 35% for most of the cases). This has consequently a direct impact on the HRF obtained.

When giving a closer inspection to the results, it is noticed that an increase in temperature implies a higher CH_4 conversion. Due to this fact there is an increase in H_2 produced

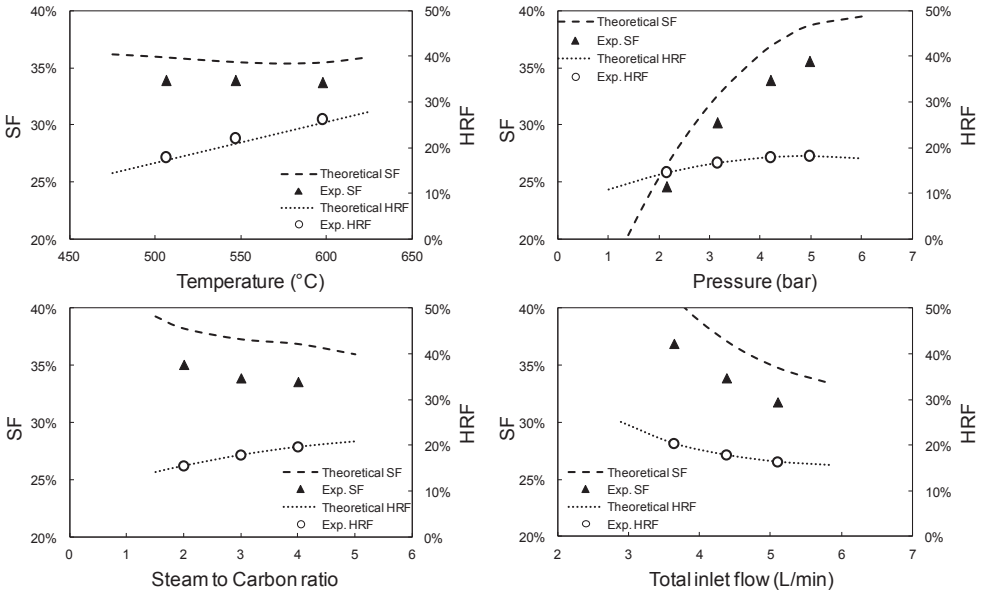

Fig. 8 – Separation Factor (SF, ▲) and Hydrogen recovery factor (HRF, o) for the different conditions studied in this work with the FBMR configuration for Steam Methane Reforming.

and hence the driving force is also increased. This increases the hydrogen permeation through the membrane with a corresponding increase in HRF. However, as more hydrogen is produced at the reactor side, the SF is not strongly affected. On the contrary, when evaluating the effect of pressure on these two parameters, there is an important increase in SF while the HRF remains almost constant. In this case, the driving force has a strong effect on the hydrogen separation factor. For low pressures, the thermodynamic equilibrium is favored to high CH_4 conversions. However, the small driving force implies a small displacement of the equilibrium with a low amount of hydrogen permeated. This explains why the SF is quite poor at such conditions. Only by working at higher pressures a more remarkable displacement of the equilibrium can be achieved resulting in a significant increase in SF and HRF.

Looking at the effect of the steam-to-carbon ratio, it is observed that for low ratios, the CH_4 conversion at equilibrium is lower, which implies lower HRF's. However, as the reaction is carried out at 4 bar, a high SF can be achieved. The contrary is obtained when increasing the steam-to-carbon ratios. The HRF is increased due to higher CH_4 conversions and due to the increase in the driving force for hydrogen separation (increase in partial pressure of H_2 at the reactor side). However, this increase in hydrogen production does not come along with a much higher increase in hydrogen permeated through the membrane with a corresponding decrease observed in the SF. Finally, the effect of residence time is also studied for this reaction. It is observed that with longer residence times the thermodynamic equilibrium can clearly be achieved, while for shorter residence times there is a small gap between the actual experimental results and the thermodynamic calculations. This is in agreement with the HRF and SF's obtained. Finally, when comparing the different figures for the CH_4 conversion and the SF, it is noticed that the small deviation to the equilibrium in CH_4 conversion for the case of the fluidized bed membrane reactor implies that also the SF deviates from the calculated equilibrium. Despite this deviation, it can be concluded that the efficiency of the reaction is almost maximized for the membrane used in this work.

Autothermal reforming of methane

Similar as for steam methane reforming, the autothermal reforming of methane has been studied for the two reactor configurations with the conditions given in Table 1. For all experiments an oxygen-to-carbon ratio of 0.25 has been selected in order to provide the heat needed to work in the autothermal regime. The procedure followed for this new process is similar as described before for SMR in the first paragraph of Section 3.3.1.

For all the cases a similar interpretation of the results can be done as for the SMR results. In the autothermal reforming case the CH_4 conversion at equilibrium is increased as a consequence of the partial oxidation with the oxygen introduced into the system. Similar to the SMR system, the thermodynamic equilibrium is almost achieved also for the autothermal reforming, as can be deduced from Fig. 9. Again, when the membrane reactor configuration is used, there is a displacement of the equilibrium as a consequence of the H_2 separation with a respective increase in the CH_4 conversion. However, as also observed in SMR process, there is a small deviation from the calculated thermodynamic equilibrium after accounting for the H_2 separated through the membrane.

For this process, the performance of the membrane is also compared in terms of the HRF and SF achieved as depicted in Fig. 10. For all conditions studied, the trends are similar as the ones described above for the SMR process. Thus the interpretation of the results given before is also valid for this new process. In the ATR process there is a small deviation in the

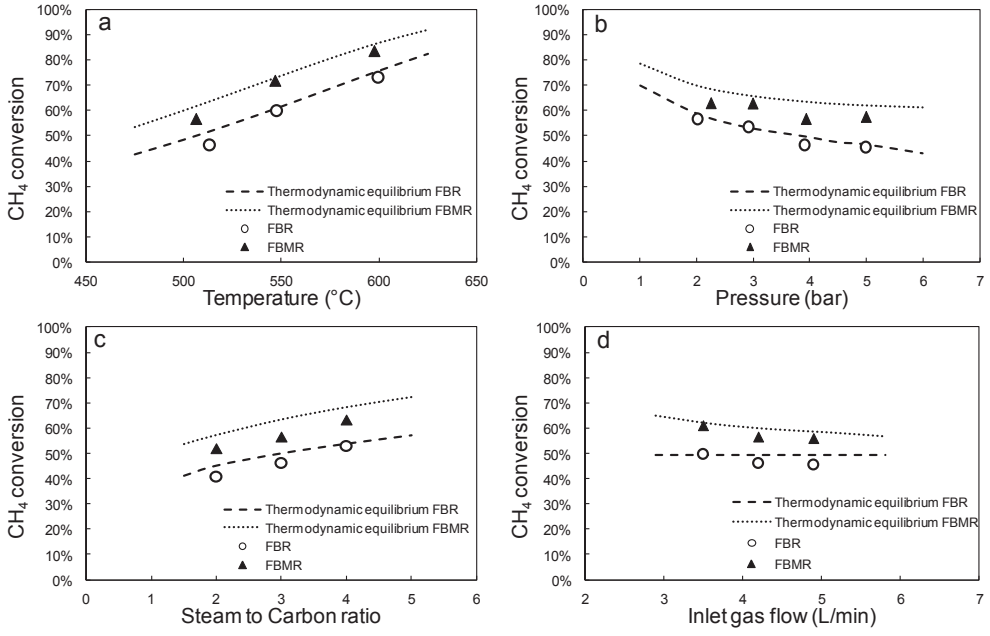

Fig. 9 – Methane conversion as a function of a) temperature, b) pressure, c) steam-to-carbon ration and d) inlet flow rate for the two reactor configurations studied with reference case conditions and the thermodynamic equilibrium for autothermal reforming of methane calculated in Aspen Plus v7.3.2.

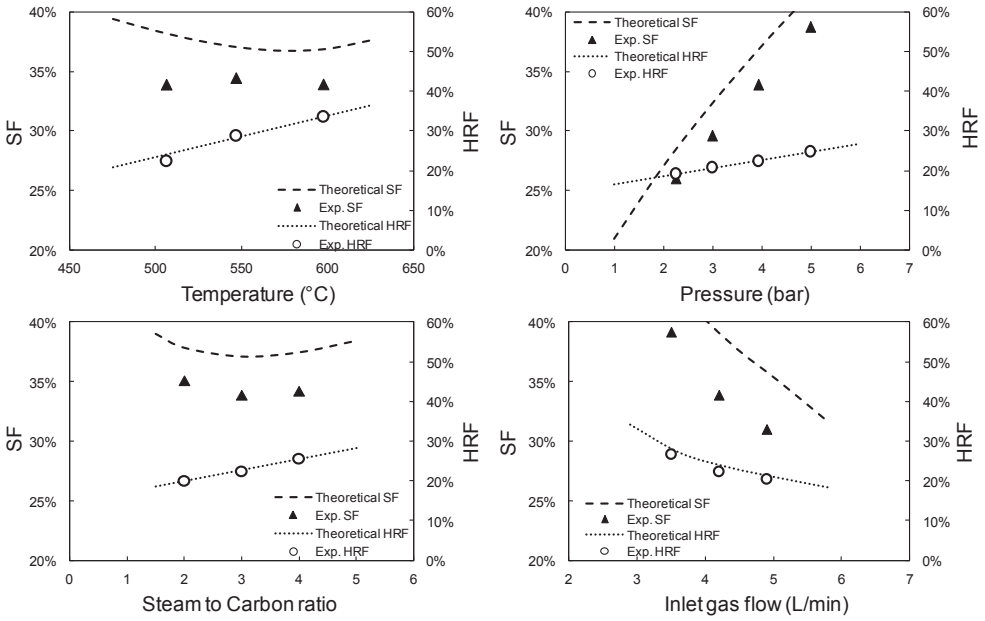

Fig. 10 – Separation Factor (SF, ▲) and Hydrogen recovery factor (HRF, o) for the different conditions studied in this work with the FBMR configuration for Autothermal Reforming of Methane.

experimental SF from the calculated equilibrium, which is also related to the small deviation observed in the CH_4 conversion.

For industrial applications it is important to restrict the concentration of CO in a H_2 stream. Thus, for both processes, the purity of the gas at the permeated side has been monitored with the analyzer. The results for some conditions are presented in Table 3. Moreover, after all experiments, the ideal H_2/N_2 perm-selectivity was calculated, which is directly correlated with the purity of the permeate stream. The results show that the membrane activity for H_2 permeation was stable after being exposed to reactive conditions, since the H_2 permeance at the same temperature was similar after every experiment. However, an important decrease in the ideal perm-selectivity is clearly observed. This decrease is directly associated to an increase in N_2 permeation through the membrane, which is explained in more detail below.

According to these results, the membrane could not be used under reaction for an industrial process since the minimum required purity was not achieved. Nonetheless, the membrane has been tested after a very long stability test where outstanding ideal perm-selectivities have been measured. If the membrane would have been used during the stability test period, it would have been possible to achieve the desired purity. However, in this work it was more important to demonstrate its stability as a function of time on stream than its performance at reactive conditions, which despite the lack of purity has shown a good behavior. Once all experiments were concluded, a deep characterization was carried out with the aim of explaining the observed decrease in the ideal perm-selectivity.

After test membrane characterization

Ethanol-helium leak test

Already at room temperature and after all the experiments at high temperature, first the defects on the membrane are analyzed by feeding helium from inside the membrane at 2 bar absolute. The permeance measured for this test was $1.38 \cdot 10^{-8}$ $mol \cdot m^{-2} \cdot s^{-1} \cdot Pa^{-1}$. On the contrary, when the membrane was submerged in ethanol, no flow through the mass flow meter nor bubbles were observed on the surface of the membrane. This indicates that all the defects come from small defects formed in the surface of the Pd layer. With this information, a more detailed characterization has been carried out.

Membrane characterization

Cross-section and surface SEM images of the tested metallic supported membrane are shown in Fig. 11. In the cross-section images (Fig. 11 a, b and c) some defects (in the range of some microns) have been observed in the membrane layer and curiously they appear on top of big metallic pores. Due to possible rearrangement of the layer after several hours of testing, defects are formed in the weak membrane part due to the low thickness of the ceramic interdiffusion barrier layer and the difficulty in covering the big surface pores of the metallic support. Fig. 11 d and e show a zone of the membrane surface where it can be seen that the Pd–Ag layer covers properly the support surface but a black zone that seems to be a hole is detected. When analyzing the black zone in Fig. 11 e by EDX (Table 4, #2) a higher concentration of the elements of the support (Al and Ni) are present compared to the continuous layer (Table 4, #1). Thus, this black zone is a defect of the Pd–Ag layer with a size in the range of the defects detected in the cross section of Fig. 11 a and b. In another zone (Fig. 11 f) a bigger defective area was detected by SEM and confirmed by EDX (Table 4, #3).

While the EDX analysis gives a good indication on the actual composition of the surface, it should still be considered as a more qualitative characterization technique than quantitative. Thus, XPS analysis is also carried out to provide more

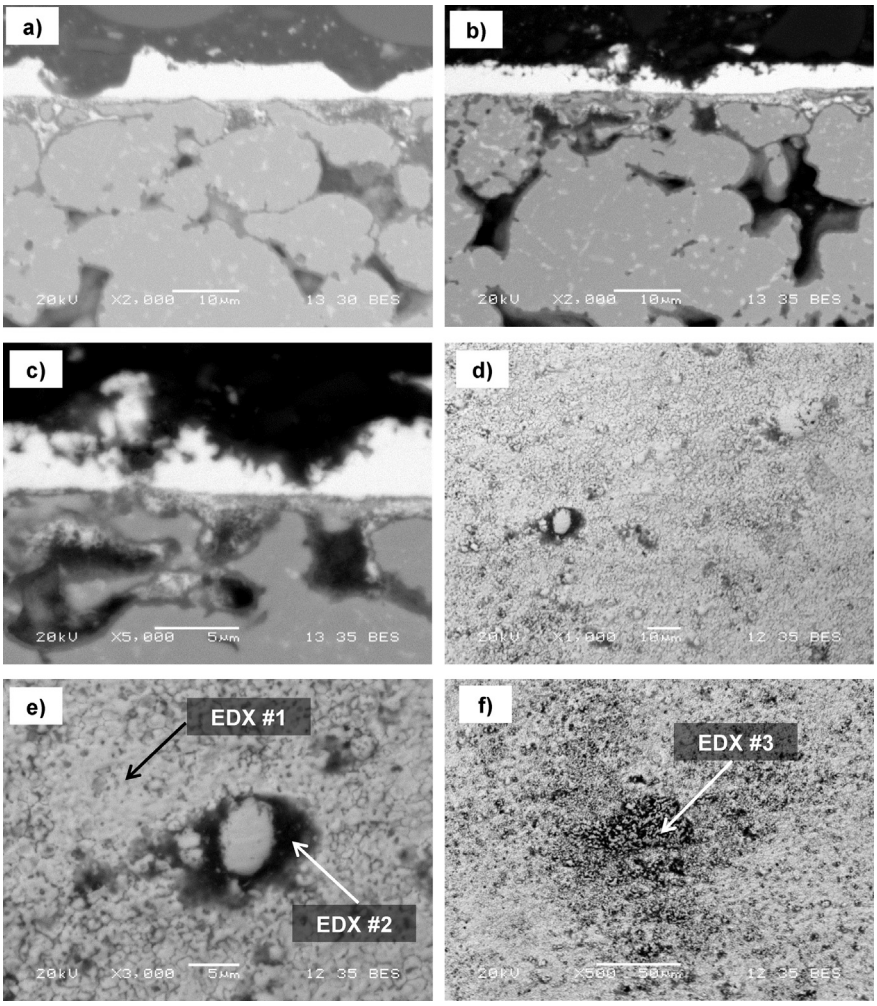

Fig. 11 – SEM pictures of the membrane after long-term and reactive tests: (a), (b) and (c) cross section images showing Pd–Ag layers with defects. (c) and (d) "zone 1" of the membrane surface where the black surrounding the particle seems to be a hole, (e) and (f) "zone 2" presenting several defects.

precise information on the composition on the membrane surface and the results have been summarized in Table 5. For a good measurement of the surface composition, first the top layer has been exposed to sputtering and thus, the measurement is done on a surface that has not been exposed to ambient conditions. Results are in agreement with the EDX measurements, where Al and Ni are clearly detected. It means that in those regions with a thin layer of ceramic barrier, there is an interaction between the support of the membrane and the top layer. This interaction results in defects on the surface, which can be related to the significant decrease in perm-selectivity observed in the long-term stability test.

Table 4 – EDX analysis results on different zones of the tested membrane presented in Fig. 11 e and f.

Spectrum	O	Al	Ni	Pd	Total
#1.- Zone "1" (Picture "d"): bright continuous layer zone 10,000x	–	–	6.86	93.14	100
#2.- Zone "1" (Picture "d"): black zone surrounding the particle 10000x	14.01	13.71	15.09	57.19	100
#3.- Zone "2" ("Picture f"): Porous/defective area 10000x	21.66	9.15	22.48	46.71	100

Conclusions

A Pd–Ag membrane (~5 μm layer) has been prepared via electroless plating and supported on metallic Hastelloy X porous tube with a ceramic layer of Al_2O_3-YSZ in between the Pd and the support in order to prevent interaction. The

Table 5 – Elementary analysis on the surface of the membrane through XPS analysis.

Sample identifier	Ag 3d %	Al 2p %	Cl 2p %	Na 1s %	Ni 2p %	Pd 3d %	Si 2p %
Before sputtering	10.84	15.35	4.37	1.58	3.89	40.84	16.97
Sputtered sample	9.48	8.74	0.99	0.53	8.23	70.87	1.16

membrane has firstly been exposed through single gas permeation tests during more than 800 h at temperatures ranging between 500 and 600 °C. During this period high H_2 permeances have been measured with exceptional high ideal selectivities always above 200,000. However, after this period, the occurrence of defects on the surface of the membrane has been observed resulting in an increase in the N_2 permeance with the consequence of a pronounced decrease in the ideal perm-selectivity. This has happened at a temperature of 600 °C, which can be considered very high for this type of membranes.

Catalyst interaction with the Pd–Ag layer has not been observed, since the H_2 permeance is the same for single gas tests in the empty tube configuration and with the fluidized bed configuration. The influence of different parameters on the membrane reactor performance has been studied for SMR and ATR reactions. In both cases the reactions were carried out first without the effect of the membrane keeping the permeate side closed. For almost all cases thermodynamic equilibrium was achieved, which was overcome when H_2 permeates through the membranes in the FBMR configuration. For this case a new steady state is created, which is again close to the calculated thermodynamic equilibrium when accounting for the H_2 extraction. After all the experiments an important decrease in the ideal H_2/N_2 perm-selectivity has been observed due to the defects created in the surface.

The explanation of the observed decrease in perm-selectivity has been carried out by means of different characterization techniques. The defects were associated to small defects formed on the surface, resulting from the interaction of the Pd layer with the metallic support. Therefore it can be concluded that this interaction could be decreased by increasing the thickness of the interdiffusion layer, possibly at the expense of a small reduction in the membrane permeance.

Acknowledgments

The presented work is funded within ReforCELL project as part of the European Union's Seventh Framework Programme (FP7/2007–2013) for the Fuel Cells and Hydrogen Joint Technology Initiative under grant agreement nº 278997 and NWO/STW for the financial support through the VIDI project number 12365. Note: "The present publication reflects only the author's views and the FCH JU and the Union are not liable for any use that may be made of the information contained therein".

The authors would like to thank Johnson Matthey for providing the catalysts. Finally, the authors would like to thank University of Basque Country (UPV-EHU) for Zabalduz scholarship program and Prof. Pedro Luis Arias.

REFERENCES

[1] IPCC. IPCC special report on carbon dioxide capture and storage. Cambridge, UK: Cambridge University Press; 2005.
[2] Rostrup-Nielsen JR. New aspects of syngas production and use. Catal Today 2000;63:159–64.
[3] Rostrup-Nielsen JR, Sehested J, Nørskov JK. Hydrogen and synthesis gas by steam- and CO_2 reforming. Academic Press; 2002. p. 65–139.
[4] Dybkjaer I. Tubular reforming and autothermal reforming of natural gas – an overview of available processes. Fuel Process Technol 1995;42:85–107.
[5] York APE, Xiao T, Green MLH. Brief overview of the partial oxidation of methane to synthesis gas. Top Catal 2003;22:345–58.
[6] Li B, Zhang S. Methane reforming with CO_2 using nickel catalysts supported on yttria-doped SBA-15 mesoporous materials via sol–gel process. Int J Hydrogen Energy 2013;38:14250–60.
[7] Angeli SD, Monteleone G, Giaconia A, Lemonidou AA. State-of-the-art catalysts for CH_4 steam reforming at low temperature. Int J Hydrogen Energy 2014;39:1979–97.
[8] Gallucci F, Sint Annaland M, Kuipers JAM. Autothermal reforming of methane with integrated CO_2 capture in a novel fluidized bed membrane reactor. Part 1: experimental demonstration. Top Catal 2008;51:133–45.
[9] Gallucci F, Sint Annaland M, Kuipers JAM. Autothermal reforming of methane with integrated CO_2 capture in a novel fluidized bed membrane reactor. Part 2 comparison of reactor configurations. Top Catal 2008;51:146–57.
[10] Medrano JA, Spallina V, van Sint Annaland M, Gallucci F. Thermodynamic analysis of a membrane-assisted chemical looping reforming reactor concept for combined H_2 production and CO_2 capture. Int J Hydrogen Energy 2014;39:4725–38.
[11] Smart S, Liu S, Serra JM, Basile A, da Costa JCD. 7-Perovskite membrane reactors: fundamentals and applications for oxygen production, syngas production and hydrogen processing. In: Gugliuzza A, Basile A, editors. Membr. clean renew. power appl. Woodhead Publishing; 2014. p. 182–217.
[12] Caravella A, Scura F, Barbieri G, Drioli E. Inhibition by CO and polarization in Pd-based membranes: a novel permeation reduction coefficient. J Phys Chem B 2010;114:12264–76.
[13] Boon J, Pieterse JAZ, van Berkel FPF, van Delft YC, van Sint Annaland M. Hydrogen permeation through palladium membranes and inhibition by carbon monoxide, carbon dioxide, and steam. J Memb Sci 2015;496:344–58.
[14] F. Gallucci A, Comite G, Capannelli A. Basile, steam reforming of methane in a membrane reactor : an industrial case study. Ind Eng Chem Res 2006;45:2994–3000.
[15] Matsumura Y, Tong J. Methane steam reforming in hydrogen-permeable membrane reactor for pure hydrogen production, top. Catal 2008;51:123–32.
[16] Peters TA, Stange M, Klette H, Bredesen R. High pressure performance of thin Pd–23%Ag/stainless steel composite membranes in water gas shift gas mixtures; influence of dilution, mass transfer and surface effects on the hydrogen flux. J Memb Sci 2008;316:119–27.
[17] Caravella A, Barbieri G, Drioli E. Concentration polarization analysis in self-supported Pd-based membranes. Sep Purif Technol 2009;66:613–24.
[18] Gallucci F, Fernandez E, Corengia P, van Sint Annaland M. Recent advances on membranes and membrane reactors for hydrogen production. Chem Eng Sci 2013;92:40–66.
[19] Deshmukh SARK, Heinrich S, Mörl L, van Sint Annaland M, Kuipers JAM. Membrane assisted fluidized bed reactors: Potentials and hurdles. Chem Eng Sci 2007;62:416–36.
[20] Roses L, Gallucci F, Manzolini G, van Sint Annaland M. Experimental study of steam methane reforming in a Pd-based fluidized bed membrane reactor. Chem Eng J 2013;222:307–20.

[21] Fernandez E, Medrano JA, Melendez J, Parco M, van Sint Annaland M, Gallucci F, et al. Preparation and characterization of metallic supported thin Pd-Ag membranes for high temperature hydrogen separation. CEJ 2015 [submitted for publication].
[22] Zeng G, Jia H, Goldbach A, Zhao L, Miao S. Hydrogen-induced high-temperature segregation in palladium silver membranes. Phys Chem Chem Phys 2014;16:25330–6.
[23] Okazaki J, Ikeda T, Pacheco-Tanaka DA, Llosa Tanco MA, Wakui Y, Sato K, et al. Importance of the support material in thin palladium composite membranes for steady hydrogen permeation at elevated temperatures. Phys Chem Chem Phys 2009;11:8632–8.
[24] Yakabe H, Kurokawa H, Shirasaki Y, Yasuda I. Operation of palldium membrane reformer system for hydrogen production: the case of Tokio Gas. In: Palladium membr. technol. hydrog. prod. carbon capture other appl; 2015. p. 311.
[25] Abu El Hawa HW, Paglieri SN, Morris CC, Harale A, Way JD. Application of a Pd–Ru composite membrane to hydrogen production in a high temperature membrane reactor. Sep Purif Technol 2015;147:388–97. 16, 2015.
[26] Guazzone F, Ma YH. Leak growth mechanism in composite Pd membranes prepared by the electroless deposition method. AIChE J 2008;54:487–94.
[27] Medrano JA, Hamers HP, Williams G, van Sint Annaland M, Gallucci F. $NiO/CaAl_2O_4$ as active oxygen carrier for low temperature chemical looping applications. Appl Energy 2015;158:86–96.
[28] Pacheco Tanaka DA, Llosa Tanco MA, Niwa S, Wakui Y, Mizukami F, Namba T, et al. Preparation of palladium and silver alloy membrane on a porous α-alumina tube via simultaneous electroless plating. J Memb Sci 2005;247:21–7.
[29] Fernandez E, Helmi A, Coenen K, Melendez J, Viviente JL, Pacheco Tanaka DA, et al. Development of thin Pd–Ag supported membranes for fluidized bed membrane reactors including WGS related gases. Int J Hydrogen Energy 2015;40:3506–19.
[30] Gallucci F, Chiaravalloti F, Tosti S, Drioli E, Basile A. The effect of mixture gas on hydrogen permeation through a palladium membrane: experimental study and theoretical approach. Int. J. Hydrogen Energy 2007;32:1837–45.
[31] Miguel CV, Mendes A, Tosti S, Madeira LM. Effect of CO and CO_2 on H_2 permeation through finger-like Pd–Ag membranes. Int J Hydrogen Energy 2012;37:12680–7.
[32] Narusawa K, Hayashida M, Kamiya Y, Roppongi H, Kurashima D, Wakabayashi K. Deterioration in fuel cell performance resulting from hydrogen fuel containing impurities: poisoning effects by CO, CH4, HCHO and HCOOH. JSAE Rev 2003;24:41–6.